

Original citation:

Zhang, Li, Gao, Weiguo, Zhang, Dawei and Tian, Yanling. (2016) Prediction of dynamic milling stability considering time variation of deflection and dynamic characteristics in thin-walled component milling process. Shock and Vibration, 2016. 3984186.

Permanent WRAP URL:

<http://wrap.warwick.ac.uk/94051>

Copyright and reuse:

The Warwick Research Archive Portal (WRAP) makes this work of researchers of the University of Warwick available open access under the following conditions.

This article is made available under the Creative Commons Attribution 4.0 International license (CC BY 4.0) and may be reused according to the conditions of the license. For more details see: <http://creativecommons.org/licenses/by/4.0/>

A note on versions:

The version presented in WRAP is the published version, or, version of record, and may be cited as it appears here.

For more information, please contact the WRAP Team at: wrap@warwick.ac.uk

Research Article

Prediction of Dynamic Milling Stability considering Time Variation of Deflection and Dynamic Characteristics in Thin-Walled Component Milling Process

Li Zhang,¹ Weiguo Gao,¹ Dawei Zhang,¹ and Yanling Tian^{1,2}

¹Key Laboratory of Mechanism Theory and Equipment Design of Ministry of Education, Tianjin University, Tianjin 300072, China

²School of Engineering, University of Warwick, Coventry CV4 7AL, UK

Correspondence should be addressed to Weiguo Gao; gaowg@tju.edu.cn

Received 4 December 2015; Accepted 21 February 2016

Academic Editor: Georges Kouroussis

Copyright © 2016 Li Zhang et al. This is an open access article distributed under the Creative Commons Attribution License, which permits unrestricted use, distribution, and reproduction in any medium, provided the original work is properly cited.

The milling stability of thin-walled component is an important problem in the aviation manufacturing industry. The milling stability is influenced by both deflection characteristic and dynamic characteristic of workpiece. Moreover, in the material removal, the deflection and dynamic characteristics of workpiece are time-variant on the change of machining positions. Thus, the milling stability is also time-variant. In order to investigate the time variation of deflection and dynamic characteristics of workpiece, a new computational model was established in this paper. Based on the influences of the deflection and the dynamic characteristics of workpiece, a new stability lobes diagram which can show different stability domains and chatter domains in different process positions was obtained. Experimental testing has been conducted to validate the established new model.

1. Introduction

Milling of thin-walled components is of great importance in aerospace, military, energy, and shipbuilding industries. Thin-walled components should be machined very carefully; otherwise they may adversely affect the performance of the whole systems. Unfortunately thin-walled parts generally have complex structure and often demonstrate unwanted deflection, instability, and vibration during machining process. In the past decades, many attempts have been made to reduce machining errors. The research results show that it is important to combine advanced control techniques and appropriately choose milling parameters to obtain high machining accuracy. Due to the complexity and difficulty in finding appropriate parameters, high quality thin-walled component milling is considered as one of the challenging problems in the manufacturing sectors. Recently, this subject has attracted many attentions of researchers who emphasize scientific predictions of the manufacturing results using computational models rather than pure experiments [1–4].

A major problem which prohibits obtaining high productivity and quality is the chatter effect which leads to the chatter marks, and such an effect may be prominent issue for high-speed and high-precision milling processes. If a machining system begins to chatter under special parameters, it will become a chatter system. The studies on chatter systems were carried out in 1960s; Tobias [5], Tlustý and Poláček [6], and Merritt [7] explained the regenerative chatter in orthogonal cuttings and developed a stability lobe theory for a two-dimensional case. The stability lobe theory aims to solve the stability boundary problems for dynamic cutting systems, which in a basic form can be usually characterized by a two-dimensional chart representing the relationship between spindle speed and axial cutting depth. Since the boundary between a stable cut and an unstable cut can be visualized in such a chart, it is called stability lobes diagram (SLD). In the middle of the 1990s, Altintas [8] presented a new analytical form of the stability lobe theory for milling. The developed stability lobe theories help select appropriate spindle speed and axial cutting depth to avoid chatter in milling processes.

More recently, several research efforts have been directed towards obtaining the SLD of a chatter system with consideration of the change of cutting position and the changes of workpiece mass and stiffness during the milling process. For instance, Bravo et al. [9] and Herranz et al. [10] considered the dynamic parameters variation of thin-walled components in a milling process as both the mass and the rigidity of the workpiece were reduced continuously. Sequentially, a three-dimensional SLD with a third axis of processing stages to cover all the intermediate stages for machining a thin wall was constructed. Schmitz et al. [11] considered the variation of system dynamics with respect to the tool overhang length and developed a three-dimensional SLD with a third axis of tool overhang lengths. Moreover, a three-dimensional SLD with a third axis of radial cutting depth for machining a thin wall was constructed by Tang and Liu [12]. An integration of dynamic behaviour variations in the stability lobes method was presented by Thevenot et al. [13]; the method was applied to thin-walled structure milling. A method for predicting simultaneous dynamic stability limit of thin-walled workpiece high-speed milling process is described by Song [14]; the proposed approach takes into account the variations of dynamic characteristics of workpiece with the tool position and a dedicated thin-walled workpiece representative of a typical industrial application is designed and modeled by finite element method.

However, milling is a material removal process. The deflection and dynamic characteristics of workpiece are time-variant and the milling stability is influenced not only by modal parameter but also by deflection which can induce the variation of immersion angle. When the stiffness of the tool and that of the workpiece are similar, the coupling deflection of workpiece must be considered.

A new computational model to investigate the time variation of deflection and dynamic characteristics is presented and a new SLD is obtained in this paper.

The paper is organized as follows: the introduction of methodology is presented in Section 2. The time-variant model of deflection and dynamic characteristics of workpiece is established in Section 3. The calculated method of milling stability is presented in Section 4. Case study and experimental verification are provided in Section 5, followed by conclusions in Section 6.

2. Methodology

Deflection and chatter phenomena of workpiece are common in milling process for thin-walled components. Actually, in milling process, the variation of immersion angle (difference between exit angle and start angle) is induced by deflection, and the immersion angle is a crucial parameter to calculate the milling force which influences the milling stability directly. Thus, deflection also has an influence on milling stability. On the other hand, the milling stability is influenced by dynamic characteristics of workpiece. In the material removal, the deflection and dynamic characteristics of workpiece are time-variant in different process positions.

A new computational model to investigate the time variation of deflection and dynamic characteristics is presented in

this paper. The finite element models (FEM) of workpiece are established. The milling process is divided into some units by tool positions. The deflection of workpiece is induced by the milling force which loads on the tool and workpiece at tool position. Since the spindle speed is high, the deflection on the unit and that on the tool position are approximately equal. Then the milling force which loads on the next tool position is induced by the deflection on the unit, and the deflection on the next unit is induced by the milling force and by this analogy. Due to the stiffness characteristics of workpiece material, the milling force loads on each tool position and the deflection of each unit is different.

The material removal rate of each unit is decided by the coupling deflection of each unit; as a result, the residual thicknesses of the different units are different. The dynamic characteristics of workpiece are time-varying with the change of tool positions and stiffness of workpiece. The SLD is not shown by one stability boundary curve, but it is shown by more curves. The stability domain and chatter domain are changed with the change of tool position.

The new SLD is obtained with the computational flow of SLD shown in Figure 1. In step 1, the initial milling force is calculated by initial milling parameters. In step 2, the deflections of workpiece on the nodes at first tool position are calculated; then the average deflection of workpiece at first tool position is obtained. In step 3, the actual radial depth of cutting at first tool position is calculated, and the start angle and the exit angle are also calculated. In step 4, the thickness of the first finished workpiece unit is calculated. In step 5, the FRF of workpiece is calculated after the first milling stage. In step 6, the modal parameters of workpiece are extracted from the FRF of workpiece. In step 7, the milling stability is calculated by modal parameters, start angle and exit angle. Then, the stability lobes diagram of first milling stage is obtained. In step 8, repeat the operations from step 1 to step 7 to calculate the milling stability of the next milling stage. After the milling process is completed, the calculation procedure will stop, where m is the number of tool positions. n is the number of nodes on contact locations of tool and workpiece. M is the sum of tool positions and N is the sum of nodes on contact locations of tool and workpiece.

3. Time-Varying Model of Deflection and Dynamic Characteristics of Workpiece

3.1. Calculations of Milling Force and Deflection. The milling process is shown in Figure 2. The workpiece can be simplified into cantilever plate, because the structural stiffness and clamping stiffness of spindle, tool, and fixture are larger enough. Thus, in the finite element models, the bottom of the workpiece is fixed.

Moreover, the nodes on contact locations of tool and workpiece are matched together. At the end of milling process, the stiffness of the thin-walled plate in the thickness direction (Y -direction) is significantly smaller than that in the feed direction (X -direction), so the deflections of tool and workpiece in the feed direction are ignored. At a certain time of milling, the milling forces acting on

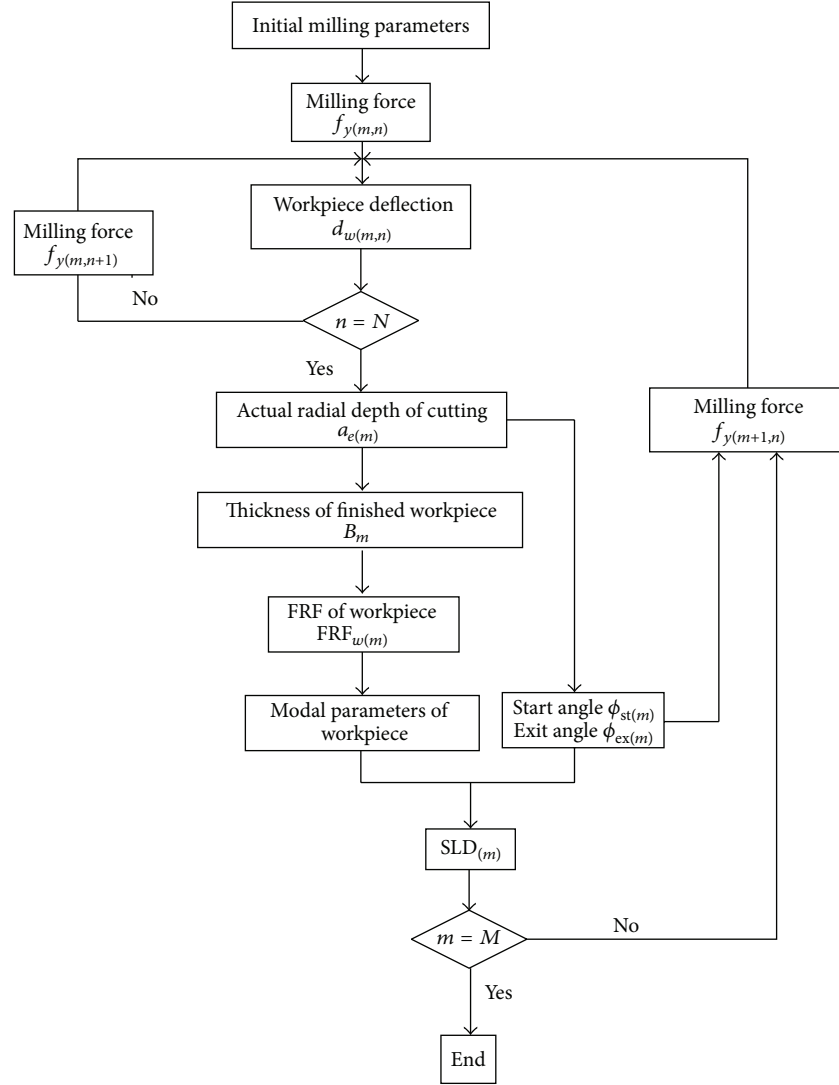


FIGURE 1: Computational flow of SLD.

the workpiece are linearly distributed along the helix direction of cutting edge. Actually, in the milling process of thin-walled components, the radial cutting depth is small and the contact time of cutting edge and workpiece is extremely short because the cutting speed is high. In order to simplify the calculation, the direction is supposed to be straight from the bottom to the top at each contact position of tool and workpiece. As shown in Figure 3, the submilling forces load on the central points of every portion of the contact locations.

According to the modeling method of milling force which is presented by Engin and Altintas [15], the angular position of infinitesimal element i on tooth j is defined as follows:

$$\phi_j = \phi_0 + (j-1)\phi_p - \frac{idz \tan \beta}{R}, \quad (1)$$

where $\phi_0 = 2\pi n_s t / 60$ and $\phi_p = 2\pi / N_c$.

The thickness of milling changes with the variety of the angular positions of cutting edge can be calculated by

$$h(\phi_j) = f_t \sin \phi_j. \quad (2)$$

Differential tangential and radial cutting forces acting on the infinitesimal of tooth j are given by

$$\begin{aligned} dF_{tj} &= g(\phi_j) [K_t h(\phi_j) + K_{te}] dz, \\ dF_{rj} &= g(\phi_j) [K_r h(\phi_j) + K_{re}] dz, \end{aligned} \quad (3)$$

where

$$g(\phi_j) = \begin{cases} 1 & \text{if } \phi_{st} < \phi_j < \phi_{ex} \\ 0 & \text{otherwise.} \end{cases} \quad (4)$$

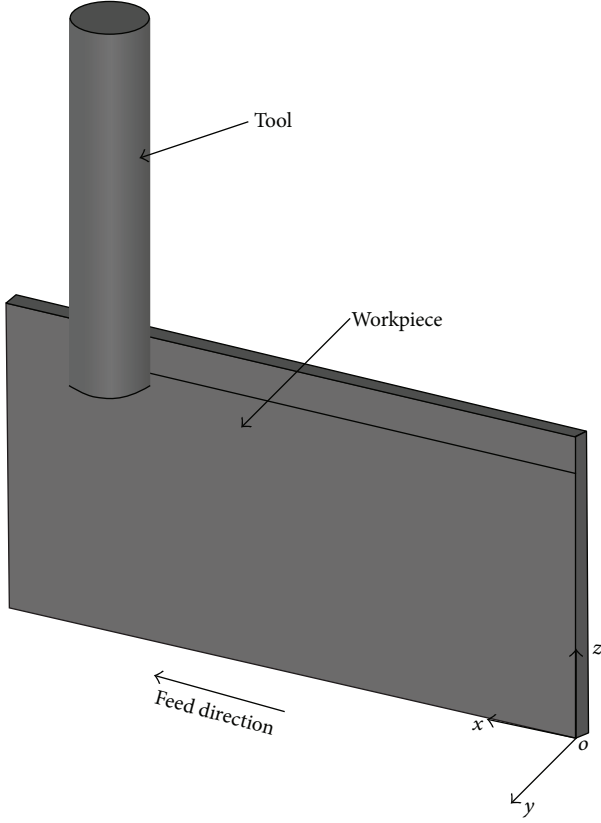


FIGURE 2: Schematic diagram of milling process.

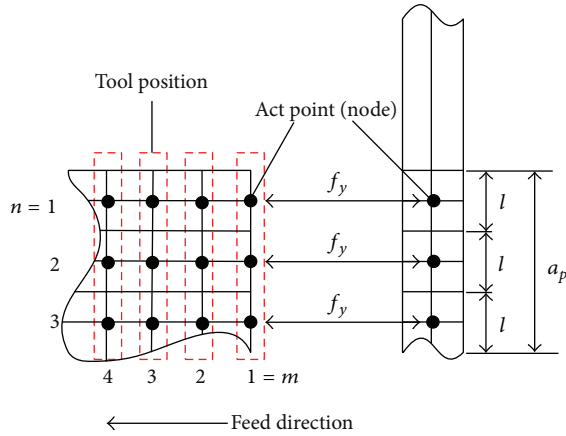


FIGURE 3: Loading locations of submilling forces.

The start angle and exit angle under up-milling and down-milling can be separately expressed by

$$\begin{aligned} \phi_{st} &= 0, \\ \phi_{ex} &= \arccos \left[1 - \frac{a_{e(m)}}{R} \right], \end{aligned} \quad (\text{up-milling}),$$

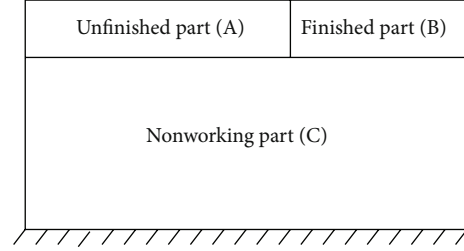


FIGURE 4: Divided parts of workpiece.

$$\begin{aligned} \phi_{st} &= \pi - \arccos \left[1 - \frac{a_{e(m)}}{R} \right], \\ \phi_{ex} &= \pi, \end{aligned} \quad (\text{down-milling}). \quad (5)$$

The deflection of workpiece is induced by milling force, and the actual radial depth of cutting at tool position m can be expressed by

$$a_{e(m)} = a_e - \frac{\left(\sum_{n=1}^N d_{w(m,n)} \right)}{N}. \quad (6)$$

It is noted that $d_{w(1,n)}$ are obtained by the initial force calculated with the nominal radial depth of cutting.

The milling force acting on the infinitesimal of tooth j and the submilling force acting on the whole cutting edges, which participate in cutting, are given as follows:

$$\begin{aligned} dF_{yj} &= dF_{ij} \sin \phi_j - dF_{rj} \cos \phi_j, \\ F_y &= \sum_{j=1}^{N_c} \sum_{i=1}^{M_c} dF_{yj}. \end{aligned} \quad (7)$$

Thus, the submilling forces acting on the central points of every portion of the contact locations can be obtained by

$$f_{y(m,n)} = \frac{l}{a_p} \cdot F_y. \quad (8)$$

3.2. Calculations of Thickness of Milling Unit. The workpiece element is divided into three parts (Figure 4): unfinished part (A), finished part (B), and nonworking part (C); the thicknesses of A and C are always initial thickness. The part of workpiece which needs milling is divided into $m - 1$ units by m tool positions (see Figure 5), and the whole milling process is divided into $m - 1$ corresponding submilling processes. The units which participate in the milling are composed for B, and other units are for A.

In milling of thin-walled components, small milling force is required to avoid the deflection and chatter; the milling parameters (radial cutting depth and feed rate per tooth) are usually small. In order to improve machining efficiency, spindle speed is set to be high. Under the high cutting speed, the variation of the deflections of workpiece is not

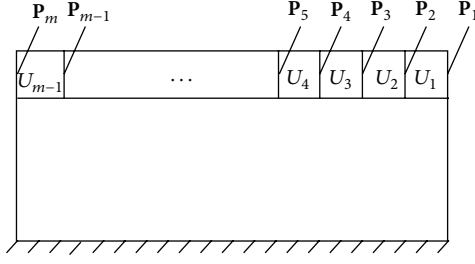


FIGURE 5: Milling units and tool positions.

obvious in a short distance. So, suppose that the deflection on the unit and that on the tool position are approximately equal.

The deflection of workpiece in the submilling process is induced by milling force, and the milling force in the next submilling process is reversely induced by the deflection of workpiece, and so on. The time variation of deflection is represented by the changes of deflections with the changes of submilling processes or tool positions. So, the thicknesses of units are different under the interaction between the milling forces and the deflections.

The thickness of each unit can be obtained by the following equation:

$$B_m = \begin{cases} B_0 & m = 1 \\ B_0 - a_e - \frac{(\sum_{n=1}^N d_{w(m,n)})}{N} & m \neq 1. \end{cases} \quad (9)$$

3.3. Time Variation of Dynamic Characteristics of Workpiece.

The dynamic characteristics of workpiece can be represented by time-variant FRF of workpiece which describes the dynamic characteristics in the range of frequency domain. The displacement of workpiece is induced by the milling force acting on the workpiece. The transfer function of workpiece can be expressed by the ratio between the displacement and milling force.

In the material removal, the stiffness characteristics of workpiece material and the loading position are changing. Thus, the FRFs of workpiece are time-variant. Consider

$$G_{y(w)}(t) = \frac{\delta_{y(w)}(t)}{F(t)}. \quad (10)$$

The relationship between the modal mass and the modal damping is satisfied:

$$m(t) = \frac{c(t)}{2\zeta(t)\omega_n(t)}, \quad (11)$$

where $\zeta(t) = c(t)/[2(m(t)k(t))^{1/2}]$, $\omega_n(t) = [k(t)/m(t)]^{1/2}$, and the values of $m(t)$, $c(t)$, and $k(t)$ can be extracted from FRF.

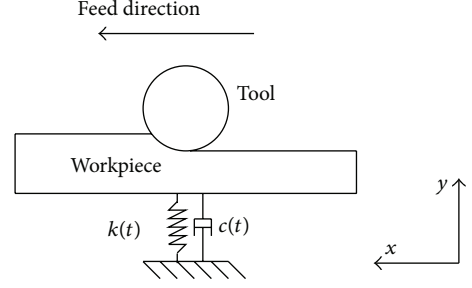


FIGURE 6: Dynamic milling model of workpiece.

4. Milling Stability of Workpiece

The initial dynamic equation can be established according to the dynamic milling model of workpiece shown in Figure 6. Consider

$$m(t)\ddot{y}(t) + c(t)\dot{y}(t) + k(t)y(t) = F(t). \quad (12)$$

Moreover, the dynamic equation of system can also be expressed as follows [16]:

$$m(t)\ddot{y}(t) + c(t)\dot{y}(t) + k(t)y(t) = -a_p h_{yy}(t) [y(t) - y(t - \tau)]. \quad (13)$$

The delayed term $y(t - \tau)$ arises due to the regenerative effect. The time delay is equal to the tooth passing period. The specific cutting force coefficient $h_{yy}(t)$ is determined by the technological parameters:

$$h_{yy}(t) = \sum_{j=1}^{N_c} g(\phi_j(t)) \sin \phi_j(t) \cdot [-K_t \sin \phi_j(t) + K_r \cos \phi_j(t)]. \quad (14)$$

From the viewpoint of dynamical systems, thin-walled workpiece can be defined as the system in which the dynamic characteristics change depending on the tool position, that is, the system considering the effect of machining process on the dynamic characteristics. The thin-walled workpiece milling process is a time-variable parameters system, and the correspondence to the governing equation has the form

$$\ddot{y}(t) + 2\zeta(t)\omega_n(t)\dot{y}(t) + \omega_n^2(t)y(t) = \frac{F(t)}{m(t)}. \quad (15)$$

Semidiscretized technique is a well-known approximation technique in FEA or in computational fluid mechanics for solving partial differential equations where the spatial coordinates are discretized while the time coordinates are unchanged [14, 17, 18]. The method can be used to determine the stability of nonautonomous approximation of the monodromy matrix Φ of a periodic delay differential equation (DDE) over the principal period T . Hereto, the period T is divided into k intervals of length Δt . The DDE is thereby approximated by a series of ordinary differential

TABLE I: Geometrical parameters of workpiece.

Category	Length (mm)	Breadth (mm)	Height (mm)	Density (g/cm ³)	Poisson's ratio	Elastic modulus (GPa)
Workpiece	100	3	50	2.7	0.33	69

equations. The convergence of the method was established for a large class of DDEs appearing in engineering applications [18, 19].

The first step of semidiscretization is the construction of the time interval division $[t_j, t_{j+1}]$ of length Δt , $j \in N$, of the time domain, so that $T = k\Delta t$, where the integer k is called approximation number. By decreasing Δt , that is, by increasing the approximation number k , the error decreases [18].

Introduce the integer m so that

$$m = \text{int} \left(\frac{\tau}{\Delta t} + 0.5 \right), \quad (16)$$

where m is an approximation parameter regarding the length of the time delay. Details on how to treat this case can be found in [18].

In the j th interval for periodic time T , the periodic DDE (15) can be approximated with the following autonomous ordinary differential equation:

$$\begin{aligned} y(t) + 2\zeta\omega_{n,j}y(t) + \left(\omega_{n,j}^2 + a_p \frac{d_j}{m_j} \right) y(t) \\ = a_p \frac{d_j}{m_j} y_{\tau,j}, \end{aligned} \quad (17)$$

where $y_{\tau,j} = \alpha y_{j-m+1} + \beta y_{j-m} \approx y(t_j + 0.5\Delta t - \tau) = y(t - \tau)$, $\omega_{n,j} = (1/\Delta t) \int_{t_j}^{t_{j+1}} \omega_n(t) dt$, $d_j = (1/\Delta t) \int_{t_j}^{t_{j+1}} d(t) dt$, and $m_j = (1/\Delta t) m(t) dt$.

By Cauchy transformation, (17) is written in the canonical form

$$\dot{\mathbf{Q}}(t) = \mathbf{W}_j \mathbf{Q}(t) + \mathbf{V}_j \left[\alpha \mathbf{Q}_{j-m+1} + \beta \mathbf{Q}_{j-m} \right], \quad (18)$$

where $\alpha = \tau/\Delta t + 0.5 - m$, $\beta = m + 0.5 - \tau/\Delta t$, $\mathbf{W}_j = \begin{bmatrix} -(\omega_{n,j}^2 + a_p(d_j/m_j)) & 1 \\ 2\zeta\omega_{n,j} & 0 \end{bmatrix}$, $\mathbf{Q}(t) = \begin{Bmatrix} y(t) \\ \dot{y}(t) \end{Bmatrix}$, $\mathbf{V}_j = \begin{bmatrix} a_p(d_j/m_j) & 0 \\ 0 & 0 \end{bmatrix}$, and $\mathbf{Q}_j = \mathbf{Q}(t_j) = \begin{Bmatrix} y(t_j) \\ \dot{y}(t_j) \end{Bmatrix} = \begin{Bmatrix} y_j \\ \dot{y}_j \end{Bmatrix}$.

For a given initial condition \mathbf{Q}_j , (18) can be solved in $t \in [t_j, t_{j+1}]$:

$$\mathbf{Q}_{j+1} = \mathbf{A}_j \mathbf{Q}_j + \mathbf{B} \left[\alpha \mathbf{Q}_{j-m+1} + \beta \mathbf{Q}_{j-m} \right], \quad (19)$$

where $\mathbf{A}_j = \exp(\mathbf{W}_j \Delta t)$, $\mathbf{B}_j = (\exp(\mathbf{W}_j \Delta t) - \mathbf{I}) \mathbf{A}_{j-1} \mathbf{V}_j$, and \mathbf{I} denotes identity matrix.

According to (19), a discrete map can be defined:

$$\mathbf{z}_{j+1} = \mathbf{P}_j \mathbf{z}_j, \quad (20)$$

where the $(m+2)$ -dimensional state vector \mathbf{z}_j is

$$\mathbf{z}_j = \begin{bmatrix} y_j & \dot{y}_j & y_{j-1} & \cdots & y_{j-m} \end{bmatrix}^T. \quad (21)$$

And the coefficient matrix \mathbf{P}_j has the form

$$\mathbf{P}_j = \begin{bmatrix} A_{j,11} & A_{j,12} & 0 & \cdots & 0 & \alpha B_{j,11} & \beta B_{j,11} \\ A_{j,21} & A_{j,22} & 0 & \cdots & 0 & \alpha B_{j,21} & \beta B_{j,21} \\ 1 & 0 & 0 & \cdots & 0 & 0 & 0 \\ 0 & 0 & 1 & \cdots & 0 & 0 & 0 \\ \vdots & \vdots & \vdots & \ddots & \vdots & \vdots & \vdots \\ 0 & 0 & 0 & 0 & 1 & 0 & 0 \\ 0 & 0 & 0 & 0 & 0 & 1 & 0 \end{bmatrix}. \quad (22)$$

Equation (20) makes the connection between states at time t_j and t_{j+1} . The connection between the states at t_0 and $t_0 + k\Delta t = t_k$ is given by coupling of the coefficient matrices in each interval:

$$\Phi = \mathbf{P}_{k-1} \mathbf{P}_{k-2} \cdots \mathbf{P}_1 \mathbf{P}_0. \quad (23)$$

The stability of (15) can be approximated by the Floquet transition matrix (see (23)). Note that the integer k determines the number of matrices to be multiplied in (23), and m determines the size of these matrices.

In one milling process, generally, the maximum displacement occurs at the top of the workpiece, and the corresponding modal shape is first-order bending modal shape of the workpiece. The modal shapes of higher modes are not effective modal shapes. So, using the semidiscretization method [16], the SLD can be obtained by first-order modal parameters as shown in Figure 7. The green zone is chatter domain and the white section is stable domain.

5. Case Study and Experimental Verification

5.1. Numerical Simulation. The geometrical parameters of workpiece are shown in Table 1. The numerical simulations are carried out with the following milling parameters in Table 2.

The simulation results under the axial milling depth of 6 mm are set as an example. As Figure 8 shows, in the milling process, the values of actual radial depth of cutting are different at different tool positions, and the trend of change of that is increased firstly and then decreases. The range abilities of changes are large at the positions of cutting in ($X = 0$ mm) and cutting out ($X = 100$ mm). The range abilities of changes are small at the positions closing to the central regions of workpiece ($X = 35$ – 65 mm). The changes of actual radial depth of cutting at tool positions are induced by deflections of workpiece. The value of actual radial depth of cutting at tool position $X = 0$ mm is the smallest because the workpiece is impacted by the milling force.

In material removal process, the stiffness of workpiece is changing and the dynamic characteristics of workpiece

TABLE 2: Parameters of milling process.

Item	Value
K_t (N/m ²)	5.403×10^8
K_r (N/m ²)	1.81×10^8
K_{te} (N/m)	2884
K_{re} (N/m)	1407
N	3
a_p (mm)	4/6/8
a_e (mm)	0.2
R (mm)	3
v (mm/min)	1200
Milling method	Down-milling

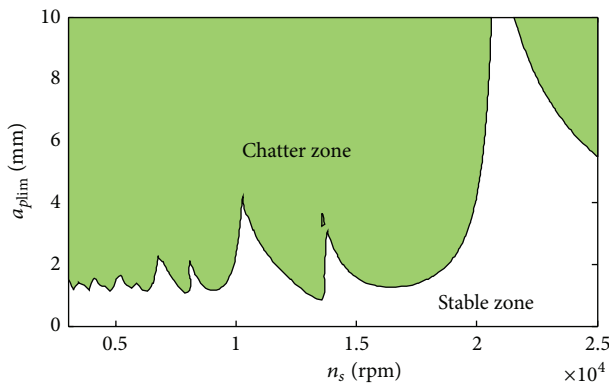


FIGURE 7: SLD of milling process.

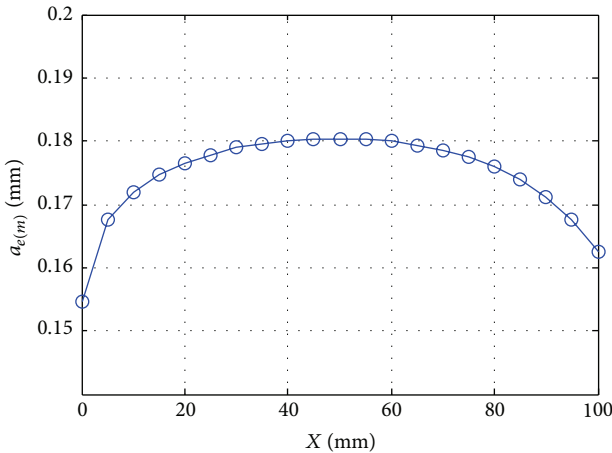


FIGURE 8: Change of actual radial depth at different tool positions.

are time-varying; the corresponding values are different at different tool positions as Figure 9 shows. The FRF of workpiece will change corresponding to the changing of the tool positions (see Figure 9(a)) and the first-order natural frequency of workpiece has changed in the range from 1045 Hz to 1056 Hz (see Figure 9(b)). The values increased firstly and then decreased with the changes of tool positions. At the same

time, the trend of change of dynamic stiffness at first mode increased firstly and then decreased (see Figure 9(c)). The stiffness of workpiece is large in the center parts and small in the boundary parts. The trends shown in Figure 9 are conformed to the stiffness characteristics of workpiece.

The dynamic milling SLD of workpiece with the axial milling depth of 6 mm are shown in Figures 10(a)–10(c), where the dots with colors in the figures represent the combination of milling parameters. If the red dot is in the stable zone, the milling process is stable under the corresponding combination of milling parameters. If the red dot is in the chatter zone, the milling process is not stable under the corresponding combination of milling parameters. The boundary curves of milling stability move upwards in the right direction with the decrease of deflection and the increases of frequency and minimum dynamic stiffness. Adversely, the boundary curves of milling stability move downwards in the left direction with the increase of deflection and the decreases of frequency and the minimum dynamic stiffness. The stable domain and chatter domain are changing with the milling steps in X-direction under the influences of the time variation of deflection and dynamic characteristics.

The same laws of change are shown in the dynamic milling SLD of workpiece with the axial milling depth of 4 mm and 8 mm (see Figures 10(d)–10(f) and 10(g)–10(i)). The ranges of stable domain and chatter domain under different combinations of milling parameters are shown in Table 3.

5.2. Experimental Verification. The milling processing is carried out by Makino S56 vertical machining center. Kistler 9257B dynamometer is used to measure the milling force and the sampling period of force test is 0.0001 s. The chatter marks on workpiece surface are observed by KEYENCE VHX-1000E super depth of field camera and the photographs are taken with 20x enlargement. The milling experimental equipment is shown in Figure 11. The material of workpiece is aluminum alloy 7075 and that of tool is cemented carbide.

Chatter marks on workpiece surface and the test signals of milling force are shown in Figure 12. The length of workpiece is 100 mm, and that of each segment photograph of chatter marks on workpiece surface is 10 mm. It is noted that the deep colors shown in photographs do not represent any meaning and are just caused by reflecting light.

The separation distance between any two adjacent chatter marks on the surface of workpiece is large and the change of amplitudes of milling force is obvious at the axial milling depth of 4 mm and spindle speed of 4000 rpm. The whole milling process is in chatter condition (see Figure 12(a)).

At the axial milling depth of 4 mm and spindle speed of 8000 rpm, the range of stable domain is 0–26.5 mm and the corresponding period of time is 0–1.325 s. In the stable domain, the separation distance between any two adjacent chatter marks on the surface of workpiece is small and the change of amplitudes of milling force is not obvious. In the period of time from 1.325 s to 4.5 s, the amplitudes of milling force and the corresponding separation distance between any

TABLE 3: Ranges of stable domain and chatter domain under different combinations of milling parameters.

Axial milling depth (mm)	Spindle speed (rpm)	Range of stable domain (mm)	Range of chatter domain (mm)
4	4000	—	0–100
	6000	—	0–100
	8000	0–25, 95–100	25–95
6	4000	5–95	0–5, 95–100
	6000	—	0–100
	8000	0–100	—
8	4000	0–100	—
	6000	0–100	—
	8000	0–100	—

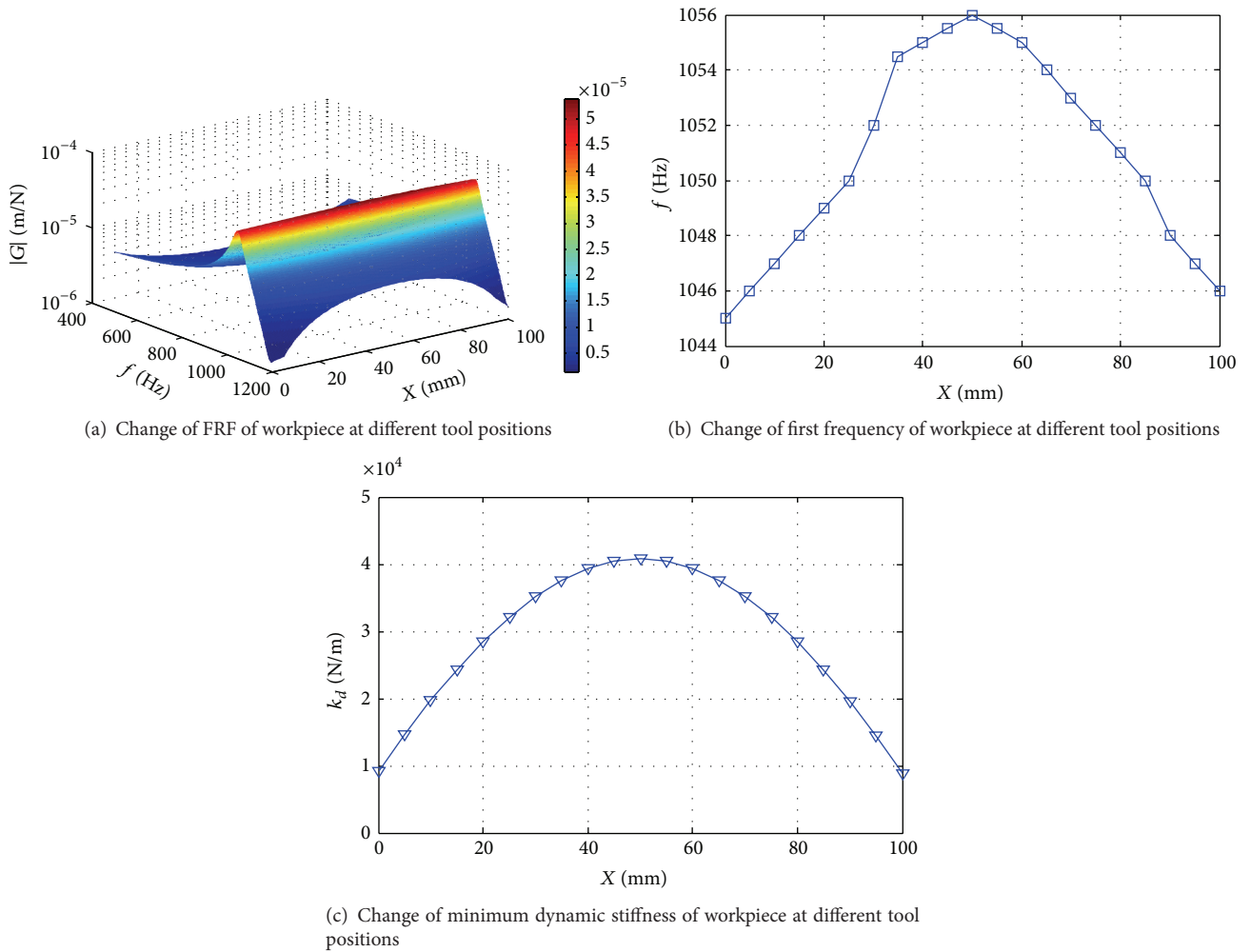


FIGURE 9: Change of dynamic characteristics of workpiece at different tool positions.

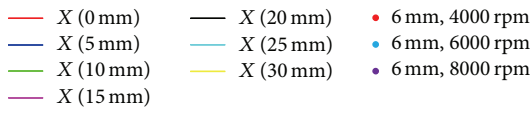
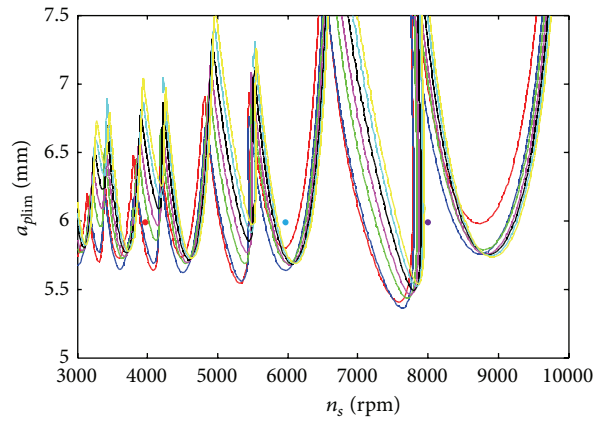
two adjacent chatter marks on the surface of workpiece are getting large obviously. In the period of time from 4.5 s to 5 s, the amplitudes of milling force are getting smaller gradually but are larger than those in the first period of time. The separation distance between any two adjacent chatter marks on the surface of workpiece is still large. So, the range of chatter domain is 26.5–100 mm (see Figure 12(b)). The chatter in range of 26.5–90 mm is obvious and that in range of 90–100 mm is not obvious.

At the axial milling depth of 6 mm and spindle speed of 8000 rpm, the separation distance between any two adjacent chatter marks on the surface of workpiece is homogeneous and the change of amplitudes of milling force is not obvious. The whole milling process is stable (see Figure 12(c)).

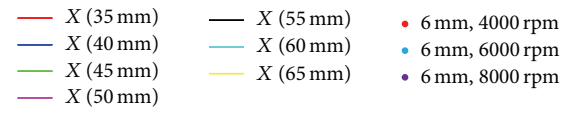
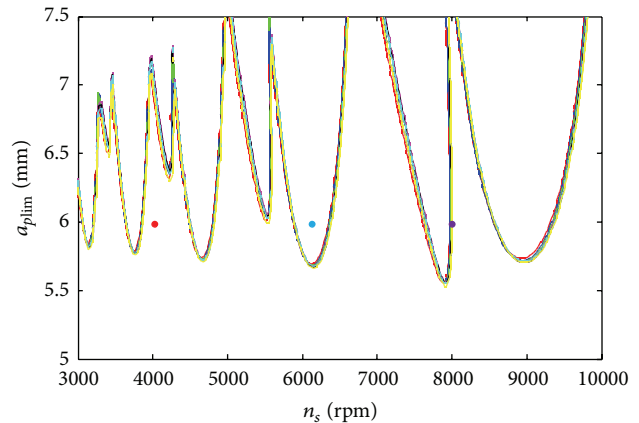
In the comparisons of ranges of stable domain and chatter domain between simulation and experiment shown in Table 4, two results are in good agreement. Thus, correctness of the established modeling method can be verified.

TABLE 4: Comparisons of ranges of stable domain and chatter domain between simulation and experiment.

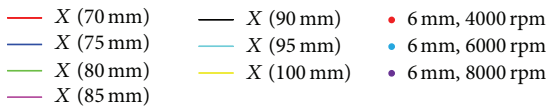
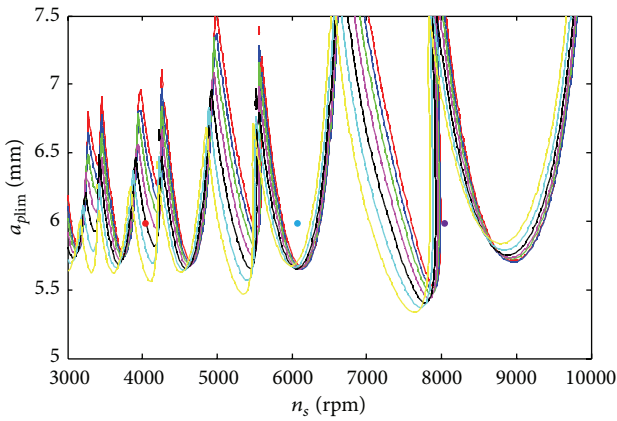
Axial milling depth (mm)	Spindle speed (rpm)	Range of stable domain of simulation (mm)	Range of stable domain of experiment (mm)	Range of chatter domain of simulation (mm)	Range of chatter domain of experiment (mm)
4	4000	—	—	0–100	0–100
	8000	0–25, 95–100	0–26.5	25–95	26.5–90 (obvious), 90–100 (not obvious)
6	8000	0–100	0–100	—	—



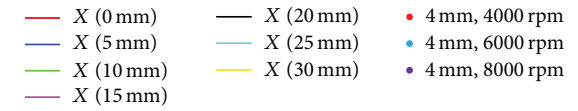
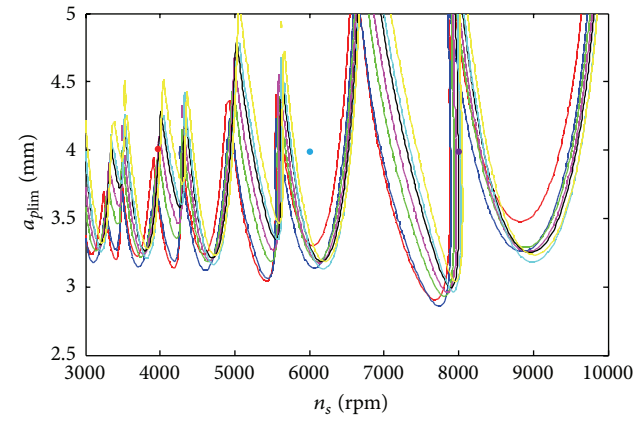
(a) Axial milling depth of 6 mm, X = 0–30 mm



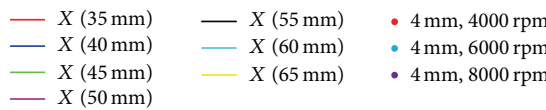
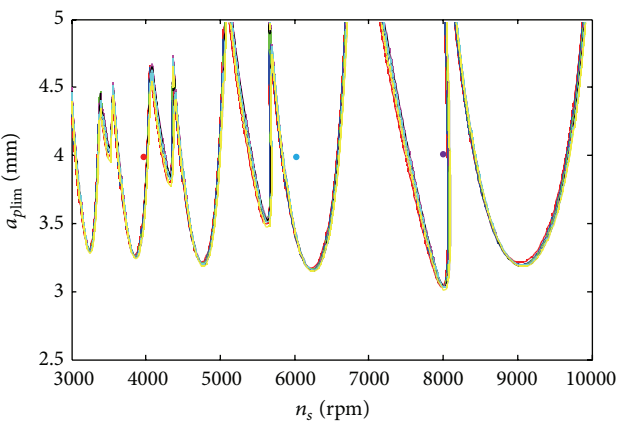
(b) Axial milling depth of 6 mm, X = 35–65 mm



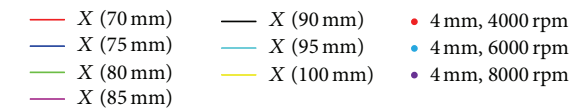
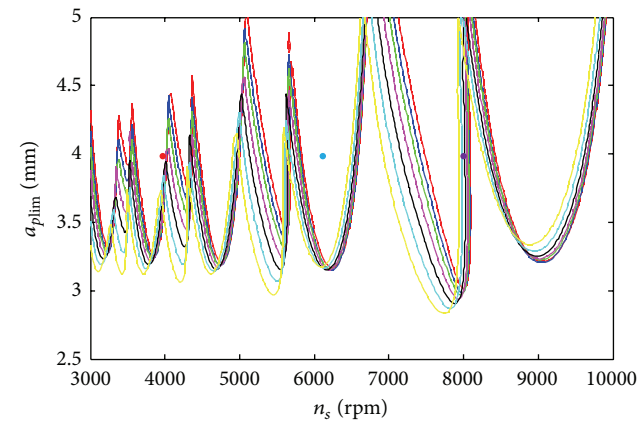
(c) Axial milling depth of 6 mm, X = 70–100 mm



(d) Axial milling depth of 4 mm, X = 0–30 mm



(e) Axial milling depth of 4 mm, X = 35–65 mm



(f) Axial milling depth of 4 mm, X = 70–100 mm

FIGURE 10: Continued.

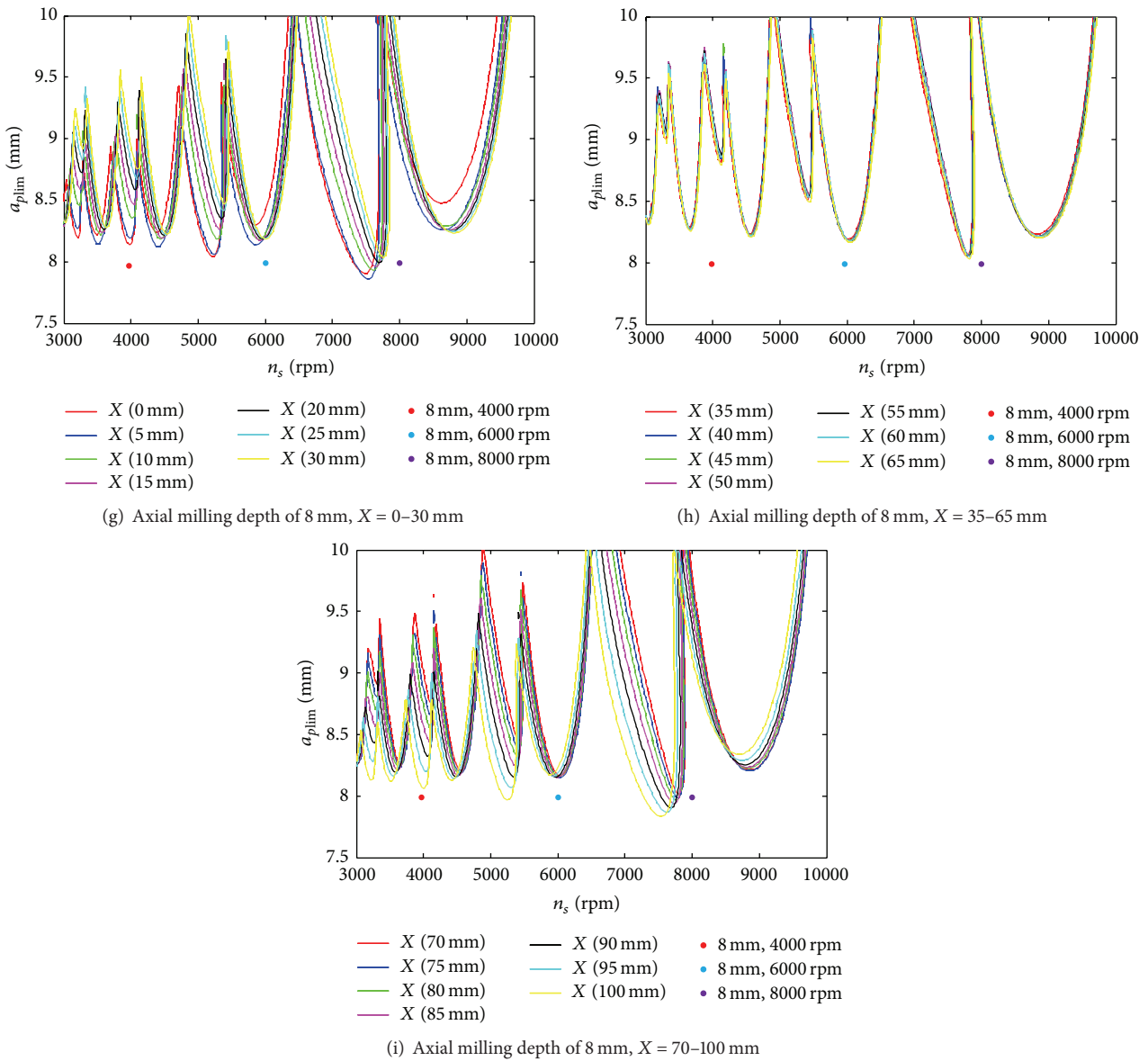


FIGURE 10: Dynamic SLD of milling process with the axial milling depth of 4 mm, 6 mm, and 8 mm.

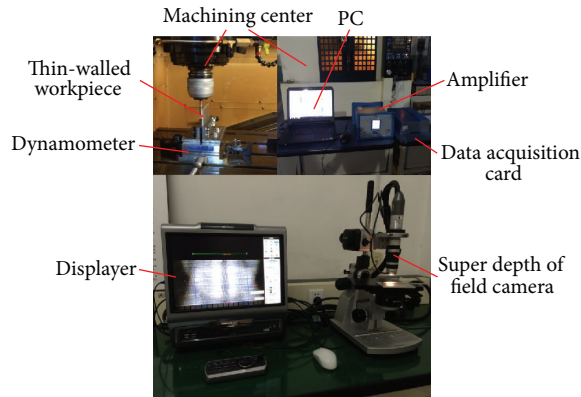
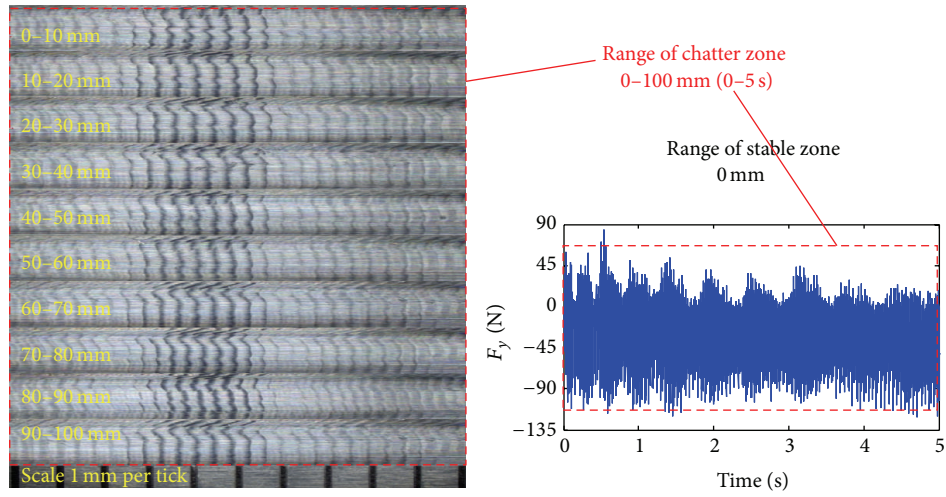
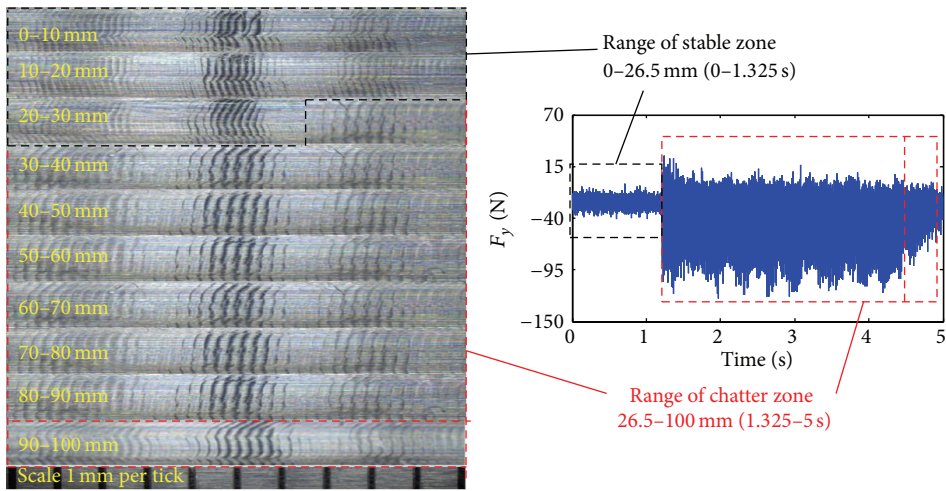


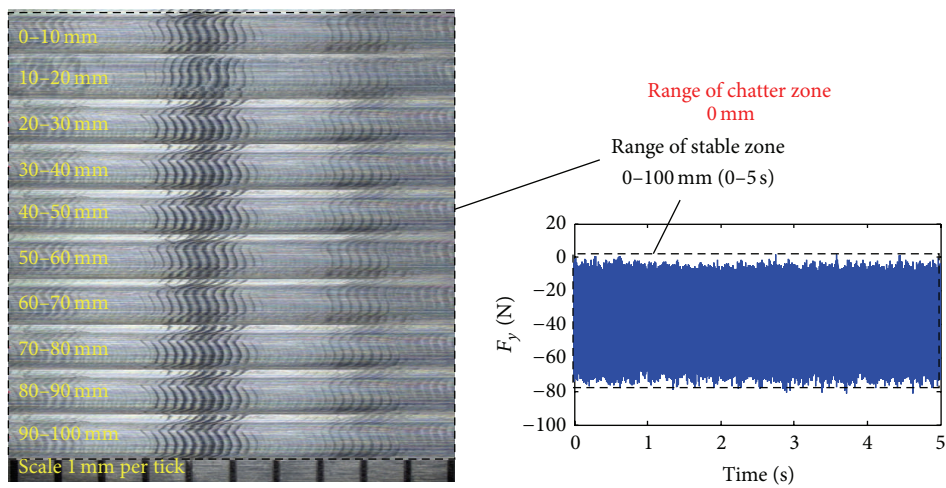
FIGURE 11: Milling experimental equipment.



(a) Axial milling depth of 4 mm and spindle speed of 4000 rpm



(b) Axial milling depth of 4 mm and spindle speed of 8000 rpm



(c) Axial milling depth of 6 mm and spindle speed of 8000 rpm

FIGURE 12: Chatter marks on workpiece surface and the test signals of milling force.

6. Conclusions

Chatter has always been a significant problem in thin-walled milling, which is one of the major limitations on productivity and part quality. In order to avoid chatter, the appropriate cutting parameters need to be selected through the stability lobe. In this paper, a new SLD has been presented. The time-varying deflection and dynamic characteristics of workpiece have been considered in the new SLD. This method is based on the identification of the optimal pairs of axial depth of cut and spindle speed at different tool position. The model approaches the actual milling process and has been demonstrated correctly by milling experiment.

Nomenclature

ϕ_j :	Angular position of tooth j ($^\circ$)
ϕ_0 :	Initial angular position of tooth j ($^\circ$)
n_s :	Spindle speed (rpm)
t :	Time (s)
j :	Number of tool teeth
ϕ_p :	Pitch angle ($^\circ$)
i :	Number of infinitesimal elements on the cutting edge
dz :	Height of infinitesimal element on the cutting edge (mm)
β :	Helical angle of tool ($^\circ$)
R :	Radius of tool (mm)
N_c :	Sum of tool teeth
$h(\phi_j)$:	Cutting thickness (mm)
f_t :	Tooth feed rate (mm/tooth)
dF_{tj} :	Differential tangential cutting force acting on tooth j (N)
dF_{rj} :	Differential radial cutting force acting on tooth j (N)
$g(\phi_j)$:	Screen function ($g(\phi_j) = 1$ denotes cutting and $g(\phi_j) = 0$ denotes no cutting)
K_t :	Tangential milling force coefficient (N/m^2)
K_r :	Radial milling force coefficient (N/m^2)
K_{te} :	Tangential linear-edge milling force coefficient (N/m^2)
K_{re} :	Radial linear-edge milling force coefficient (N/m^2)
ϕ_{st} :	Start angle ($^\circ$)
ϕ_{ex} :	Exit angle ($^\circ$)
m :	Number of tool positions
n :	Number of nodes on contact locations of tool and workpiece
$a_{e(m)}$:	Actual radial depth of cutting at tool position m (mm)
$d_{w(m,n)}$:	Deflection of workpiece at node n and tool position m (mm)
dF_{yj} :	Differential milling force in Y -direction of tooth j (N)
F_y :	Milling force in Y -direction (N)
M_c :	Sum of differential elements on the cutting edge
$f_{y(m,n)}$:	Submilling force loading on the central points in every portion of the contact locations (N)

l :	Length of every portion (mm)
a_p :	Axial depth of cutting (mm)
a_e :	Nominal radial depth of cutting (mm)
M :	Sum of tool positions
N :	Sum of nodes on contact locations of tool and workpiece
B_0 :	Initial thickness of workpiece (mm)
B_m :	Thickness of unit (mm)
$G_{y(w)}(t)$:	Transfer function of workpiece with time variation in Y -direction (mm/N)
$\delta_{y(w)}(t)$:	Displacement of workpiece with time variation in Y -direction (mm)
$F(t)$:	Dynamic milling force (N)
$m(t)$:	Modal mass of workpiece (kg)
$c(t)$:	Modal damping of workpiece ($\text{N}\cdot\text{s}/\text{m}$)
$k(t)$:	Modal stiffness of workpiece (N/m)
$\omega_n(t)$:	Natural frequency of workpiece (Hz)
$\zeta(t)$:	Modal damping ratio of workpiece
$y(t)$:	Chatter displacement (mm).

Competing Interests

The authors declare that there are no competing interests regarding the publication of this paper.

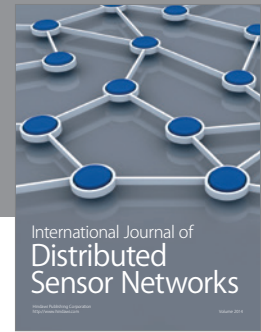
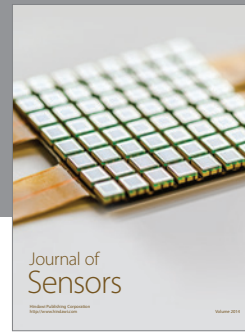
Acknowledgments

The authors acknowledge the state S&T projects for upmarket NC machine and fundamental manufacturing equipment of China (no. 2012ZX04012-031, no. 2013ZX04005-013, and no. 2015ZX04005001, resp.).

References

- [1] S. Ratchev, S. Liu, W. Huang, and A. A. Becker, "Milling error prediction and compensation in machining of low-rigidity parts," *International Journal of Machine Tools and Manufacture*, vol. 44, no. 15, pp. 1629–1641, 2004.
- [2] S. Ratchev, S. Liu, W. Huang, and A. A. Becker, "A flexible force model for end milling of low-rigidity parts," *Journal of Materials Processing Technology*, vol. 153–154, no. 1–3, pp. 134–138, 2004.
- [3] E. Budak, "Analytical models for high performance milling. Part I: cutting forces, structural deflections and tolerance integrity," *International Journal Machine Tools & Manufacture*, vol. 46, pp. 1478–1488, 2006.
- [4] J. K. Rai and P. Xirouchakis, "Finite element method based machining simulation environment for analyzing part errors induced during milling of thin-walled components," *International Journal of Machine Tools and Manufacture*, vol. 48, no. 6, pp. 629–643, 2008.
- [5] S. A. Tobias, *Machine Tool Vibration*, Blackie and Sons, London, UK, 1965.
- [6] J. Tlustý and M. Poláček, "The stability of machine Tools against self excited vibrations in machining," in *Proceedings of the ASME Production Engineering Research Conference*, pp. 465–474, 1963.
- [7] H. E. Merritt, "Theory of self-excited machine-tool chatter: contribution to machine-tool chatter research-1," *Journal of Engineering for Industry*, vol. 87, no. 4, pp. 447–454, 1965.

- [8] Y. Altintas, *Manufacturing Automation-Metal Cutting Mechanics, Machine Tool Vibrations and CNC Design*, Chemical Industry Press, 2002.
- [9] U. Bravo, O. Altuzarra, L. N. López de Lacalle, J. A. Sánchez, and F. J. Campa, “Stability limits of milling considering the flexibility of the workpiece and the machine,” *International Journal of Machine Tools and Manufacture*, vol. 45, no. 15, pp. 1669–1680, 2005.
- [10] S. Herranz, F. J. Campa, L. N. López de Lacalle et al., “The milling of airframe components with low rigidity,” *Proceedings of the Institution of Mechanical Engineers, Part B: Journal of Engineering Manufacture*, vol. 219, no. 11, pp. 789–801, 2005.
- [11] T. L. Schmitz, T. J. Burns, J. C. Ziegert, B. Dutterer, and W. R. Winfough, “Tool length-dependent stability surfaces,” *Machining Science and Technology*, vol. 8, no. 3, pp. 377–397, 2004.
- [12] A. Tang and Z. Liu, “Three-dimensional stability lobe and maximum material removal rate in end milling of thin-walled plate,” *International Journal of Advanced Manufacturing Technology*, vol. 43, no. 1-2, pp. 33–39, 2009.
- [13] V. Thevenot, L. Arnaud, G. Desein, and G. Cazenave-Larroche, “Integration of dynamic behaviour variations in the stability lobes method: 3D lobes construction and application to thin-walled structure milling,” *International Journal of Advanced Manufacturing Technology*, vol. 27, no. 7-8, pp. 638–644, 2006.
- [14] Q. Song, X. Ai, and W. Tang, “Prediction of simultaneous dynamic stability limit of time-variable parameters system in thin-walled workpiece high-speed milling processes,” *International Journal of Advanced Manufacturing Technology*, vol. 55, no. 9-12, pp. 883–889, 2011.
- [15] S. Engin and Y. Altintas, “Mechanics and dynamics of general milling cutters. Part I: helical end mills,” *International Journal of Machine Tools & Manufacture*, vol. 41, no. 15, pp. 2195–2212, 2001.
- [16] T. Insperger and G. Stépán, “Updated semi-discretization method for periodic delay-differential equations with discrete delay,” *International Journal for Numerical Methods in Engineering*, vol. 61, no. 1, pp. 117–141, 2004.
- [17] T. Insperger, B. P. Mann, G. Stépán, and P. V. Bayly, “Stability of up-milling and down-milling. Part I. Alternative analytical methods,” *International Journal of Machine Tools & Manufacture*, vol. 43, no. 1, pp. 25–34, 2003.
- [18] T. Insperger and G. Stépán, “Semi-discretization method for delayed systems,” *International Journal for Numerical Methods in Engineering*, vol. 55, no. 5, pp. 503–518, 2002.
- [19] F. Hartung, T. Insperger, G. Stépán, and J. Turi, “Approximate stability charts for milling processes using semi-discretization,” *Applied Mathematics and Computation*, vol. 174, no. 1, pp. 51–73, 2006.



Hindawi

Submit your manuscripts at
<http://www.hindawi.com>

